Resolution of Carvedilol's Conformational Surface via Gas and Solvent Phase Density Functional Theory Optimizations and NMR Spectroscopy

David R. P. Almeida,*,†,‡ Donna M. Gasparro,†,§ Tamás A. Martinek,‡,⊥ Ferenc Fülöp,‡,∥ and Imre G. Csizmadia*,†,#,○

Department of Chemistry, Lash Miller Chemical Laboratories, University of Toronto, 80 St. George Street, Toronto, Ontario, Canada M5S 3H6, Institute of Pharmaceutical Chemistry, University of Szeged, Eötvös u. 6., H-6720 Szeged, Hungary, and Department of Medicinal Chemistry, University of Szeged, Dom ter 8, 6720 Szeged, Hungary

Received: April 29, 2004

The pharmaceutical carvedilol acts as a nonselective β (β_1/β_2) and selective α (α_1) adrenoceptor antagonist, cardioprotector, antioxidant, oxidative phosphorylation uncoupler, and amyloid-β (Aβ) antifibrillar agent. Given these diverse pharmacodynamic profiles, the resolution of carvedilol's highly populated conformations are necessary to divulge the basis of its interactions with these molecular targets. However, given carvedilol's sizable conformational hypersurface (11 torsional angles and 3^{11} conformational possibilities), this task is preferentially achieved by means of a novel rational molecular fragmentation method to minimize computational and experimental resources. Presently we have isolated and optimized nine low energy carvedilol conformers with high level B3LYP/6-31G(d) density functional theory (DFT with the Becke 3LYP hybrid exchange-correlation functional) molecular orbital computations in the gas phase and in the solvent phase (DMSO and water) with Onsager solvent reaction field calculations as a means to arrive at the uncharacterized low energy structures and solvent effect of carvedilol. Additionally, carvedilol has been analyzed with NMR spectroscopy (in DMSO) to correlate theoretical- and experimental-derived electronic structure. Gas phase results show that seven of the nine conformers possess a novel tetracentric spiro-type conformation composed of intramolecular six- and eight-membered rings. This structural motif is dictated by the necessary stabilization of the positively charged nitrogen group and by the inflexibility of the carbazole aromatic ring. DMSO and water DFT optimizations and NMR spectroscopy closely mirror each other indicating that carvedilol has a subtle energetic and structural solvent effect. ROESY and scalar coupling show further evidence of the rigid rotation about the large carbazole pharmacophore. Given the harmony achieved between theoretical and experimental results, this study suggests the most populated states of carvedilol expected to dominate physical and biological samples and gives credence to the ability of methodically analyzing complex molecular systems by means of theoretical structure−activity fragmentation. Together, this will critically aid the molecular understating of carvedilol's pharmacodynamic mechanisms and structural underpinnings.

1. Introduction

The cardiovascular pharmaceutical carvedilol, 1-(9*H*-carbazol-4-yloxy)-3-[2-(2-methoxy-phenoxy)ethylamino]-2-propanol ($C_{24}H_{26}N_2O_4$), is used in the treatment of hypertension, ischemic heart disease (IHD), and congestive heart failure (CHF).[1,2] Biological actions of carvedilol include the following: antagonist action at α (α_1) and β (β_1 and β_2) membrane adrenoceptors, reduction of reactive oxygen species (ROS) mediated oxidative stress, and modulator of cardiac electrophysiological properties via interaction with K^+ and Ca^{2+} ion channels.[1]

Carvedilol's hemodynamic benefits are a result of peripheral vasodilation and reduction in cardiac work from balanced nonselective β-receptor blockage (β_1 and β_2) and selective α_1-receptor blockage.[1−3] As a cardioprotector, carvedilol exerts antiproliferative/antiatherogenic, antihypertrophic, antiischemic, and antiarrhythmic actions by means of antioxidant effects, improvement of glucose and lipid metabolism, modulation of neurohormonal factors (e.g., nitric oxides), and fine-tuning of cardiac electrophysiological properties.[1] In addition, carvedilol provides further cardioprotection by protecting mitochondria from oxidative stress by uncoupling oxidative phosphorylation via a weak protonophoretic (proton transfer) mechanism involving the amino group ($pK_a = 7.9$) of its side chain.[4]

As a novel antifibrillar agent, carvedilol may have uses in the prevention or slowing down of Alzheimer's disease (AD).[5] Work has indicated that carvedilol and its active hydroxylated analogues are able to inhibit amyloid-β (Aβ) fibril formation[5] and, thus, may benefit AD patients since increased accumulation of Aβ oligomers drives AD pathogenesis.[6−11] However, possible carvedilol/Aβ interaction(s) are unknown.

Given the intricate nature of carvedilol, it is evident that revealing carvedilol's conformational profile and its highly populated conformations are indispensable to expounding the molecular basis of its mechanisms of action. However, given carvedilol's 11 associated torsional angles and 177 147 (3^{11}) conformational possibilities (the total is arrived at by means of multidimensional conformation analysis [MDCA] where each torsional angle can assume *gauche plus*, *anti*, or *gauche minus* orientations), it is clear that this is a extensive and laborious

* Corresponding author. E-mail: dalmeida@medscape.com.
† University of Toronto.
‡ Institute of Pharmaceutical Chemistry, University of Szeged.
§ E-mail: dgasparro@medscape.com.
⊥ E-mail: martinek@phanal.szote.u-szeged.hu.
∥ E-mail: fulop@pharma.szote.u-szeged.hu.
○ Department of Medicinal Chemistry, University of Szeged.
E-mail: icsizmad@alchemy.chem.utoronto.ca.

10.1021/jp0403240 CCC: $27.50
Published on Web 08/19/2004

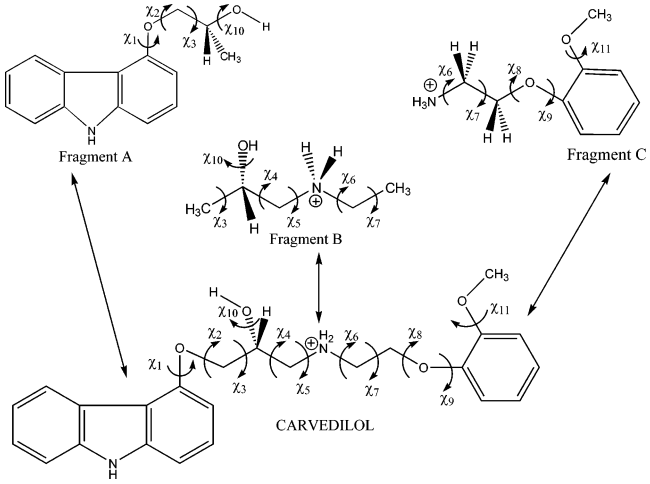

Figure 1. Carvedilol was divided into three molecular fragments based on pharmacophore structure: *R*- and *S*-4-(2-hydroxypropoxy)carbazole (fragment A),[12,15] 2(*R* and *S*)-1-(ethylamonium)propane-2-ol (fragment B),[13] and aminoethoxy-2-methoxybenzene (fragment C).[14]

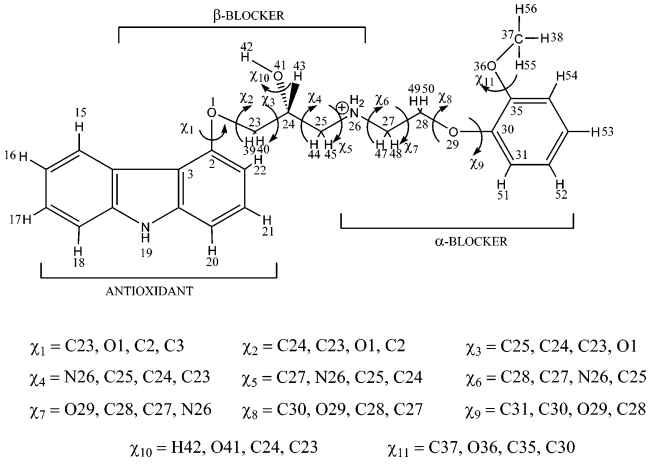

Figure 2. Molecular structure and pharmacophore structure−function of N-protonated *R*-carvedilol and all torsional angle definitions used in the current study. Numbers placed beside atoms were used to define torsional angles for *R*-carvedilol in the **z**-matrix input for Gaussian 98 and for NMR spectroscopic analysis.

task by conventional MDCA or random potential energy hypersurface (PEHS) sampling.

To remedy the above quandary, we previously developed a scheme based on the rational molecular fragmentation of pharmacophore regions to fragment the pharmacophores of carvedilol into three independent structures[12] (cf. Figure 1). All three fragments were then exhaustively optimized by MDCA,[12−14] along with thorough analysis of the chiral properties of carvedilol[15] and several hydrogen bond (H-bond) intramolecular attractive forces (IMAF).[16] The latter results were cumulatively used to predict and optimize 240 conformations hypothesized to be low energy structures.[17]

In the current study, the authors subject nine novel carvedilol low energy conformations to high level density functional theory (DFT) optimizations in gas, dimethyl sulfoxide (DMSO), and water phases and analyze carvedilol with nuclear magnetic resonance (NMR) spectroscopy to achieve a 2-fold aim: (1) discover and describe the most populated (lowest energy) states of carvedilol expected to dominate physical and biological samples and (2) analyze the success of this novel "structure−activity fragmentation" approach to the detailed theoretical study of complex molecular systems.

2. Methods

2.1. Rational Molecular Fragmentation of Carvedilol. Carvedilol is composed of three distinct pharmacophores and was divided into three molecular fragments (cf. Figure 1 and 2). Each fragment has been previously studied by the use of MDCA: *R*- and *S*-4-(2-hydroxypropoxy)carbazole (fragment A) possesses the carbazole ring responsible for the direct antioxidant effects of carvedilol,[12] 2(*R* and *S*)-1-(ethylamonium)propane-2-ol (fragment B) contains the protonophoretic amino group involved in the cardioprotective uncoupling of mitochondrial oxidative phosphorylation,[13] and aminoethoxy-2-methoxybenzene (fragment C) is the α_1-adrenergic antagonist pharmacophore of carvedilol.[14]

By optimization of a comprehensive list of 240 conformations hypothesized to be low energy carvedilol structures, an authentic set of nine distinct conformers (out of 121 converged minima) were discovered with a conformer relative energy of less than four kcal·mol^{-1} at the RHF/3-21G level of theory.[17] The dominant interaction inherent in seven of these nine conformers is a unique "tetracentric" (four-centered) spiro-type structure

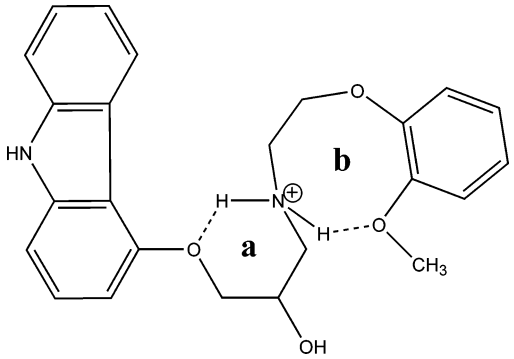

Figure 3. Schematic representation of the "tetracentric" spiro-type conformational motif exhibited by most carvedilol low energy conformations (figure adapted from reference 17). This structural motif consists of a six-membered ring (ring **a**) bonded to the terminal carbazole centroid and an eight-membered ring (ring **b**) bonded to the terminal substituted benzene. The intramolecular rings are formed by means of two short O···H−N H-bonds.

composed of two intramolecular rings (six- and eight-membered) enclosed by two O···H−N H-bonds (cf. Figure 3).[17] Overall, the rational molecular fragmentation method employed was able to predict eight of the 11 torsional angles accurately (72.7%) according to the torsional angle conformation distribution.[17]

Although the RHF/3-21G level of theory performed exceptionally well at optimizing a large number of carvedilol structures and ultimately allowing us to arrive at a set of nine structures,[17] the RHF/3-21G gas-phase calculations are not enough for full structural and energetic account of focal carvedilol conformers. Furthermore, exclusive gas-phase optimizations or solvent phase single point energy (SPE) calculations are not sufficient in of themselves because they do not allow in depth analysis of the as-of-yet uncharacterized solvent effect of carvedilol. As such, in the current article, we perform high level gas and solvent phase DFT optimizations on these nine structures and evaluate carvedilol with NMR spectroscopy as to present the conformations of carvedilol expected to preponderate gas and solvent samples. In turn, such a comparison between theoretically- and experimentally determined carvedilol structures will lead to carvedilol's conformational solution.

2.2. Carvedilol Torsional Angle Definitions. To allow explicit prediction and definition of conformation, a systematic numbering system has been used for all structures such that

corresponding torsional angles in fragments and carvedilol are all defined in the same manner (cf. Figure 2). All PEHS conformers of carvedilol can be described by eq 1. Further, conformational structural assignments for converged minima are made according to eq 2 based on the general observation that, if one were to rotate a tetrahedral carbon against another tetrahedral carbon, the minima would generally fall within the above ranges.

$$E = f(\chi_1, \chi_2, \chi_3, \chi_4, \chi_5, \chi_6, \chi_7, \chi_8, \chi_9, \chi_{10}, \chi_{11}) \quad (1)$$

$$\textit{gauche plus}\ (g^+) = 60 \quad (\text{ideal}) \pm 60^\circ \quad (2)$$

$$\textit{anti}\ (a) = 180 \quad (\text{ideal}) \pm 60^\circ$$

$$\textit{gauche minus}\ (g^-) = -60 \quad (\text{ideal}) \pm 60^\circ$$

2.3. Theoretical and Computational Methods. All structures were subject to molecular orbital (MO) optimizations using the Gaussian 98 (G98) software program.[18] Initially, full optimizations in the gas phase ($\epsilon = 0.0$) were performed using density functional theory (DFT) with the Becke 3LYP hybrid exchange-correlation functional[19] at the B3LYP/6-31G(d) level of theory (the inputs for these gas-phase DFT calculations were RHF/3-21G optimized results taken from ref 17).

Proceeding, DFT gas-phase optimized carvedilol structures were then used as input for DFT self-consistent reaction field (SCRF) optimizations to characterize the solvent effect (solvent-induced change in energy difference) of carvedilol. Independent molecular volume calculations were first computed on all gas-phase DFT converged structures to estimate a solute radius (a_0) for use with the Onsager solvent reaction field method.[20−25] Once the solute radii had been calculated, the Onsager method was utilized at the B3LYP/6-31G(d) level of theory to optimize all structures in aprotic DMSO ($\epsilon = 46.70$) and protic water ($\epsilon = 78.39$) solvents. The Onsager method places the solute in a fixed spherical cavity, defined by the solute radius, within the solvent field.[26] Net stabilization is achieved corresponding to the interactions between the molecular dipole (which induces a dipole in the solvent medium) and the electric field applied by the solvent dipole.[26] To satisfy the need of quantitatively significant results, the self-consistent field (SCF) "tight" option was utilized for volume and Onsager calculations for a more accurate integration by means of an increase in the density of points used. Graphical data was plotted using Axum 5.0[27] and Excel.[28]

2.4. Experimental NMR Spectroscopy Methods. A total of 47.7 mg of carvedilol (purchased from ChemPacific Corporation, Baltimore, MD) was dissolved in 550 μL of deuterated DMSO (DMSO-d_6) solvent. All of the spectra were obtained on a Bruker DRX 400 MHz NMR spectrometer at 298 K using tetramethylsilane (TMS) as a reference at zero parts per million (ppm). Proton chemical shifts were assigned and structural information was obtained with decoupled, COSY (correlated spectroscopy), NOESY (nuclear Overhauser enhancement spectroscopy), and ROESY (rotational Overhauser enhancement spectroscopy) spectra. Mixing time was modulated in NOESY experiments for best signal-to-noise ratio in NOE build up curves. All 2D spectra were zero filled once in both dimensions.

The reasons for choosing DMSO (DMSO-d_6) as the solvent for all NMR spectra are 3-fold: (1) DMSO is a polar solvent which generally destroys weak intramolecular H-bonds, and therefore, it is a good solvent to test the rigidity of the structure and thereby the strength of any assumed H-bond networks; (2) DMSO is an aprotic solvent preventing the $^1H-^2D$ exchange with polar protons of the solute (contrary to $CDCl_3$ or D_2O) which allows to obtain information on the chemical shifts of the OH and NH protons; (3) carvedilol NMR spectroscopy in DMSO can be promptly compared with DFT optimizations in DMSO available with the G98 software program.

3. Results and Discussion

3.1. Structural Analysis of Gas-Phase Optimized Carvedilol Conformations. According to eq 2, a summary of optimized torsional angle conformation for all converged structures of carvedilol is presented in Table 1. Upon gas-phase DFT optimization, all nine conformations possessed a gas phase relative energy of less than 2 kcal·mol^{-1} (cf. Table 2) compared with a conformer relative energy of less than 4 kcal·mol^{-1} for the previously computed RHF/3-21G structures.[17]

In concordance with the prior RHF/3-21G optimized structures, close scrutiny of these DFT low energy conformations reveals that seven (C-*R*-246 to C-*R*-250, C-*R*-258, and C-*R*-272) of the nine conformations possess the novel tetracentric spiro-type structural motif (cf. Figure 3 and 4). The tetracentric conformation is flanked on one side by the 13-membered aromatic carbazole ring (center 1) which is connected to a six-membered ring closed via an intramolecular O···H−N H-bond between the carbazole ether oxygen and a proton of the nitrogen center (ring **a**; center 2). The same protonated secondary nitrogen atom − via the other proton − forms an eight-membered ring (ring **b**; center 3) through another intramolecular O···H−N H-bond to the methoxy oxygen of carvedilol. The "right side" of the carvedilol conformation if flanked by the disubstituted benzene ring (center 4) which also forms part of ring **b**. Rings **a** and **b** are formed via short H-bonds that are in all cases less than two angstroms in length and always involves both protons of the nitrogen center (cf. Figure 4). There does not appear to be any IMAF between the amine protons and the methoxy oxygen (O36) of conformations C-*R*-251 and C-*R*-273; consequently, these conformations do not form ring **b**. In order that this tetracentric structural motif form, it is necessary that the positive protonated nitrogen center of the carvedilol side-chain is present for the concomitant formation of the two essential O···H−N H-bonds. If only one proton (in the neutral amine form) is present, instead of the positive protonated group, it is likely that it would not be possible to form rings **a** and **b**.

Aside from this tetracentric conformation, the highly populated states of carvedilol presented in Figure 4 possess various further intramolecular H-bond networks; albeit these are composed of much longer H-bonds compared to those of enclosed rings **a** and **b**. Aside from differences related to the tetracentric conformational motif, the nine low energy carvedilol structures can be divided into two groups: those with three internal H-bonds (C-*R*-246, C-*R*-247, C-*R*-251, C-*R*-258, C-*R*-272, and C-*R*-273) and those with four internal H-bonds (C-*R*-248, C-*R*-249, and C-*R*-250) (cf. Figure 4). These additional H-bonds form various intramolecular five-membered rings.

As previously evaluated,[12,17] the rational molecular fragmentation of protonated carvedilol is based on the deconstruction of carvedilol into three dominant pharmacophore fragments: a positive secondary amine side-chain (fragment B) flanked by an electron-withdrawing group (EWG) carbazole ring system (fragment A), and an EWG benzene centroid (fragment C). Given these three structural considerations, it can be rationalized that the prevalence of the tetracentric conformation in seven of the nine DFT optimized conformers is a result of stabilizing the positively charged nitrogen group. The electronic structure of this motif allows the electron-donating groups (EDG) found on the carbazole (ether oxygen bridge, O1) and benzene (methoxy oxygen, O36) rings to act as EDG to these respective

TABLE 1: Optimized Torsional Angle Orientations of the Carvedilol Structures Evaluated in the Current Study[a]

structure code	torsional angle conformation										
	χ_1	χ_2	χ_3	χ_4	χ_5	χ_6	χ_7	χ_8	χ_9	χ_{10}	χ_{11}
C-*R*-246	$[g^+/a/a/a]$	$[a/a/a/a]$	$[g^-/g^-/g^-/g^-]$	$[g^+/g^+/g^+/g^+]$	$[g^+/g^+/g^+/g^+]$	$[a/a/a/a]$	$[g^-/g^-/g^-/g^-]$	$[g^-/g^-/g^-/g^-]$	$[g^-/g^-/g^-/g^-]$	$[g^+/g^+/g^+/g^+]$	$[g^+/g^+/g^+/g^+]$
C-*R*-247	$[g^+/g^+/g^+/g^+]$	$[a/a/a/a]$	$[g^-/g^-/g^-/g^-]$	$[g^+/g^+/g^+/g^+]$	$[g^+/g^+/g^+/g^+]$	$[g^+/g^+/g^+/g^+]$	$[g^-/g^-/g^-/g^-]$	$[a/a/a/a]$	$[g^+/g^+/g^+/g^+]$	$[g^+/g^+/g^+/g^+]$	$[a/a/a/a]$
C-*R*-248	$[g^+/g^+/g^+/g^+]$	$[a/a/a/a]$	$[g^-/g^-/g^-/g^-]$	$[g^+/g^+/g^+/g^+]$	$[a/a/a/a]$	$[a/a/a/a]$	$[g^+/g^+/g^+/g^+]$	$[a/a/a/a]$	$[g^-/g^-/g^-/g^-]$	$[g^+/g^+/g^+/g^+]$	$[g^+/g^+/g^+/g^+]$
C-*R*-249	$[g^+/g^+/g^+/g^+]$	$[a/a/a/a]$	$[g^-/g^-/g^-/g^-]$	$[g^+/g^+/g^+/g^+]$	$[a/a/a/a]$	$[g^-/g^-/g^-/g^-]$	$[g^-/g^-/g^-/g^-]$	$[g^-/g^-/g^-/g^-]$	$[g^-/g^-/g^-/g^-]$	$[g^+/g^+/g^+/g^+]$	$[g^+/g^+/g^+/g^+]$
C-*R*-250	$[g^+/g^+/g^+/g^+]$	$[a/a/a/a]$	$[g^-/g^-/g^-/g^-]$	$[g^+/g^+/g^+/g^+]$	$[a/a/a/a]$	$[g^-/g^-/a/a]$	$[g^+/g^+/g^+/g^+]$	$[a/a/a/a]$	$[g^-/g^-/g^-/g^-]$	$[g^+/g^+/g^+/g^+]$	$[a/a/a/a]$
C-*R*-251	$[g^+/g^+/g^+/g^+]$	$[a/a/a/a]$	$[g^-/g^-/g^-/g^-]$	$[g^+/g^+/g^+/g^+]$	$[a/a/a/a]$	$[g^-/g^-/g^-/g^-]$	$[g^-/g^-/g^-/g^-]$	$[a/a/a/a]$	$[g^+/g^+/g^+/g^+]$	$[g^+/g^+/g^+/g^+]$	$[a/a/a/a]$
C-*R*-258	$[g^+/g^+/g^+/g^+]$	$[a/a/a/a]$	$[g^-/g^-/g^-/g^-]$	$[g^+/g^+/g^+/g^+]$	$[g^+/g^+/g^+/g^+]$	$[a/a/a/a]$	$[g^-/g^-/g^-/g^-]$	$[g^+/g^+/g^+/g^+]$	$[g^+/g^+/g^+/g^+]$	$[g^+/g^+/g^+/g^+]$	$[g^-/g^-/g^-/g^-]$
C-*R*-272	$[g^+/g^+/g^+/g^+]$	$[a/a/a/a]$	$[g^-/g^-/g^-/g^-]$	$[g^+/g^+/g^+/g^+]$	$[g^+/g^+/g^+/g^+]$	$[g^+/g^+/g^+/g^+]$	$[g^+/g^+/g^+/g^+]$	$[g^+/g^+/g^+/g^+]$	$[g^+/g^+/g^+/g^+]$	$[g^+/g^+/g^+/g^+]$	$[g^-/g^-/g^-/g^-]$
C-*R*-273	$[g^+/g^+/g^+/g^+]$	$[a/a/a/a]$	$[g^-/g^-/g^-/g^-]$	$[g^+/g^+/g^+/g^+]$	$[a/a/a/a]$	$[g^+/g^+/g^+/g^+]$	$[g^+/g^+/g^+/g^+]$	$[a/a/a/a]$	$[g^-/g^-/g^-/g^-]$	$[g^+/g^+/g^+/g^+]$	$[a/a/a/a]$

[a] Molecular conformation is displayed as [input torsional angle geometry/gas phase B3LYP/6-31G(d) optimized torsional angle geometry/DMSO solvent phase B3LYP/6-31G(d) optimized torsional angle geometry/water solvent phase B3LYP/6-31G(d) optimized torsional angle geometry]. Explicit values of torsional angles are found in Tables 2−4. Torsional angle geometries have been previously optimized at the RHF/3-21G level of theory (taken from ref 17) and are used here as input structures for DFT optimizations.

centroids, and also to the positive nitrogen group. The formation of intramolecular rings **a** and **b** facilitates an electron density redistribution process whereby the ether (O1) and methoxy (O36) EDG induct electron density into the positive nitrogen group via O···H−N H-bonds.

Although conformations C-*R*-251 and C-*R*-273 do not possess ring **b** of the tetracentric motif (cf. Figure 4), the net effect inherent in these structures is still the stabilization of the positive nitrogen group by the use of H-bonds. However, in the case of these two conformers, the O···H−N H-bonds are between amine protons and the hydroxyl oxygen (O41) and second ether oxygen (O29) leading to the formation of independent five-membered rings. In C-*R*-251 and C-*R*-273, these two intramolecular H-bonds operate to produce the similar electron induction into the nitrogen group.

Given the above, it can be concluded that although the tetracentric structural motif represents the preferred and likely most populated gas phase conformation of carvedilol, the nitrogen side-chain can be stabilized by various H-bonds that all serve the function of inducting (or redistributing) electron density into the positive nitrogen group. In total, the carvedilol intramolecular H-bond networks are composed of various H-bonds that can originate from two amine proton H-bond donors (H46 and H57) to four oxygen H-bond acceptors (O1, O29, O36, and O41).

The chemical literature available is limited with regard to the detailed description of carvedilol's gas-phase structure[12−17,29]; thus, it is difficult to compare the above DFT results with previous experimental works. The X-ray diffraction crystal structure of carvedilol, developed by Chen and co-workers,[29] utilizes the deprotonated neutral form (with respect to the side-chain nitrogen center) of carvedilol and displays a pair of carvedilol enantiomers interacting via short intermolecular O41−H42···N26 H-bonds (two H-bonds per enantiomer pair).[29] However, since the crystal displays neutral intermolecular enantiomer structure, it does not elucidate any intramolecular structural parameters of single-molecule protonated carvedilol. The bona fide structural analysis of single-molecule carvedilol performed here is relevant to carvedilol's mechanisms of action because these are a result of one *R*- or *S*-configuration molecule interacting with adrenoceptors, ROS, or Aβ peptides. As such, these single-molecule conformations of carvedilol describe the dominant structures it assumes before any solvent effect occurs and prior to complexing with such molecular targets.

3.2. Structural Analysis of DMSO and Water Phase Optimized Carvedilol Conformations. DFT optimization of carvedilol conformations in aprotic DMSO (cf. Figure 5 and Table 3) and protic water (cf. Figure 6 and Table 4) solvents were performed independently, using DFT optimized gas-phase results as input files, to bring to light carvedilol's solvent effect. A graphical representation of this solvent effect is displayed in Figure 7.

Superficially, from Figure 7, it is evident that DMSO and water solvation of carvedilol produces the same effects on structural parameters and conformer relative energy; i.e., the same solvent effect is present for both a protic and aprotic solvent as DMSO and water results produced nearly identical torsional angle and energy values. Energetically, the overall effect of the two solvents on carvedilol was the augmentation in both the relative and absolute values in all conformers except C-*R*-250 and C-*R*-273 which possessed similar relative energies in all phases (cf. Figure 7). However, the relative orientation of the conformers, with respect to one another, did not change.

Pertaining to electronic structure, torsional angle conformation distribution in Table 1 indicates that, for a respective carvedilol

TABLE 2: Gas Phase ($\epsilon = 0.0$) Optimized Values and Energies for the Converged Conformers of the Protonated *R*-Carvedilol Surface at the B3LYP/6-31G(d) Level of Theory

structure code	torsional angle (deg)											energy (Hartree)	relative energy (kcal·mol^{-1})
	χ_1	χ_2	χ_3	χ_4	χ_5	χ_6	χ_7	χ_8	χ_9	χ_{10}	χ_{11}		
C-*R*-246	147.66	−178.59	−61.82	67.01	92.56	179.24	−47.81	−68.16	−68.34	54.30	90.60	−1340.99055043	0.11
C-*R*-247	107.44	−171.16	−53.41	67.92	85.46	108.38	−51.47	146.95	106.47	56.63	177.53	−1340.98911556	1.01
C-*R*-248	100.13	−169.42	−51.87	67.66	−167.27	−168.85	65.24	−129.63	−77.61	49.02	106.78	−1340.98917601	0.98
C-*R*-249	98.69	−171.84	−51.36	71.22	−162.18	−59.94	−47.41	−71.17	−70.95	51.53	96.98	−1340.99072989	0.00
C-*R*-250	97.94	−174.38	−51.60	71.66	−170.02	−108.22	51.08	−145.73	−113.20	61.69	178.99	−1340.99052227	0.13
C-*R*-251	97.63	−172.97	−49.97	72.69	−173.97	−66.19	−46.46	175.94	112.05	55.44	179.71	−1340.98883102	1.19
C-*R*-258	97.47	−174.15	−55.86	63.28	83.88	175.26	−60.45	116.50	69.38	57.43	−88.53	−1340.98857046	1.36
C-*R*-272	92.99	−175.06	−54.27	63.77	80.27	63.58	44.88	71.86	68.43	57.95	−94.63	−1340.98826529	1.55
C-*R*-273	91.74	−177.88	−52.41	72.27	171.03	63.65	47.12	−177.41	−110.11	51.57	−177.05	−1340.98879141	1.22

conformer, torsional angle orientation was essentially consistent between RHF and DFT optimizations as well as between gas, DMSO, and water phase calculations. The latter is suggestive that these carvedilol low energy states are indeed densely populated so that only few major rearrangements between gas and solvent phases occur. In comparing parameters between gas (cf. Figure 4), DMSO (cf. Figure 5), and water (cf. Figure 6) converged conformers, the majority did not undergo any noteworthy changes. Conformers C-*R*-247 (tetracentric with three H-bonds), C-*R*-248 (tetracentric with four H-bonds), C-*R*-249 (tetracentric with four H-bonds), C-*R*-251 (no tetracentric motif with three H-bonds), C-*R*-258 (tetracentric with three H-bonds), C-*R*-272 (tetracentric with three H-bonds), and C-*R*-273 (no tetracentric motif with three H-bonds) all displayed the same conformations in gas, DMSO, and water.

The only conformers that underwent any noticeable structural changes were C-*R*-246 and C-*R*-250. Conformer C-*R*-246 rotated torsional angle χ_1 from the g^+ position (RHF results from ref 17) to the anti position in all DFT calculations (cf. Table 1). However, this χ_1 rotation only produced a slight change in orientation of the carbazole ring and did not produce any other significant structural alterations as all DFT structures still assumed the tetracentric motif. Contrasting, C-*R*-250 did undergo a significant conformational change in rotating torsional angle χ_6 from the g^- position in RHF (ref 17) and DFT gas-phase results (cf. Table 1 and 2) to the anti position in DFT DMSO and water calculations (cf. Table 3 and 4). In the gas phase, C-*R*-250 possesses the tetracentric motif with four internal H-bonds (cf. Figure 4). Nevertheless, upon the χ_6 rotation in DMSO (cf. Figure 5) and water (cf. Figure 6), this conformer rearranged such that the methoxy oxygen (O36) no longer interacted with any amine protons, and therefore, could not form ring **b** pertaining to the tetracentric structure. In the solvent phases, C-*R*-250 still possesses a short O1···H46−N H-bond but formed a much stronger O41···H57···O29 bifurcated H-bond with distances of 2.27 and 2.15 Å, respectively, in both DMSO and water (cf. Figure 5 and 6).

This structural change conferred conformer C-*R*-250 with a global minima relative energy in both DMSO and water (cf. Figure 7). This is likely due to the lack of any IMAF involving the methoxy oxygen (O36) which would allow the positive nitrogen and amine protons to be solvated by DMSO and would allow extensive solvation of the positive nitrogen group and O36 by water. Consequently, C-*R*-250 was the only carvedilol structure to display a solvent (both DMSO and water) relative energy of less than one kcal·mol^{-1} (cf. Figure 7 and Table 3 and 4).

Intuitively, it follows that the carvedilol structure will be better solvated if it lacks any IMAF as shown for conformer C-*R*-250. In such cases, it is likely that specific H-bond interactions will occur with solvent molecules, especially with regard to protic water. As such, the inability to explicitly treat solvent molecules that are directly H-bonded to the solute is a limitation of continuum solvent models such as the Onsager used here. However, given carvedilol's large size and degrees of freedom, the Onsager solvent model provides a very satisfactory method for initial geometry optimization and structural analysis of such molecules in a solvent medium.

Furthermore, given the fact that the NMR spectroscopy corroborates the same rigid structure as the solvent optimizations of carvedilol (cf. section 3.4 below), it is likely that the conformers presented here are densely populated low energy minima which favor intramolecular interaction vs solute−solvent interactions in a continuum solvent environment. In future work, we hope to use the current carvedilol solvent optimized geometries as input coordinates for solvent calculations where specific explicit solvent molecules are present (to identify specific solute−solvent H-bond interactions) while the additional bulk solvent is treated with the same Onsager solvent model.

Given the current DFT Onsager solvent reaction field calculations, carvedilol can be said to have a subtle solvent effect with regard to energetics and electronic structure. On the whole, most structures did not undergo any major structural alterations upon solvent optimization and preferred the tetracentric conformation and other IMAF related to stabilizing the carvedilol structure seen in the gas phase. It can thus be stated that the carvedilol gas phase conformations are excellent starting points for any structural or mechanistic analysis of carvedilol.

3.3. Theoretical Resolution of Carvedilol's Conformational Surface. All torsional angle orientations necessary for carvedilol to assume both the tetracentric conformational motif as well as all other IMAF presented in this communication are jointly expressed in eq 3 (forward slash "/" indicates "or"). Although the carvedilol PEHS is one of large conformational flexibility, the low energy structures presented here display unanticipated rigidity in several torsional angles; the DFT results demonstrate that 4 (χ_2, χ_3, χ_4, and χ_{10}) of the 11 torsional angles assume only one orientation. In other words, given the large number of possible conformational minima in the carvedilol PEHS, it was previously assumed that low energy minima might be sporadic across the PEHS rather than being entirely centered about a definite set of conformational assignments.

Compounding the above with the fact that all four torsional angles belong to fragment A, and torsional angle χ_1 assumes an anti conformation in only one conformer (C-*R*-246) while being g^+ in all other converged carvedilol structures, it can be hypothesized that the large carbazole-containing pharmacophore dictates (i.e., the conformation of carbazole fragment A does not change and therefore it is postulated to greatly influence) the prevalent stable conformations of the carvedilol molecule. Likewise, there is also a dominant *gauche effect* in the

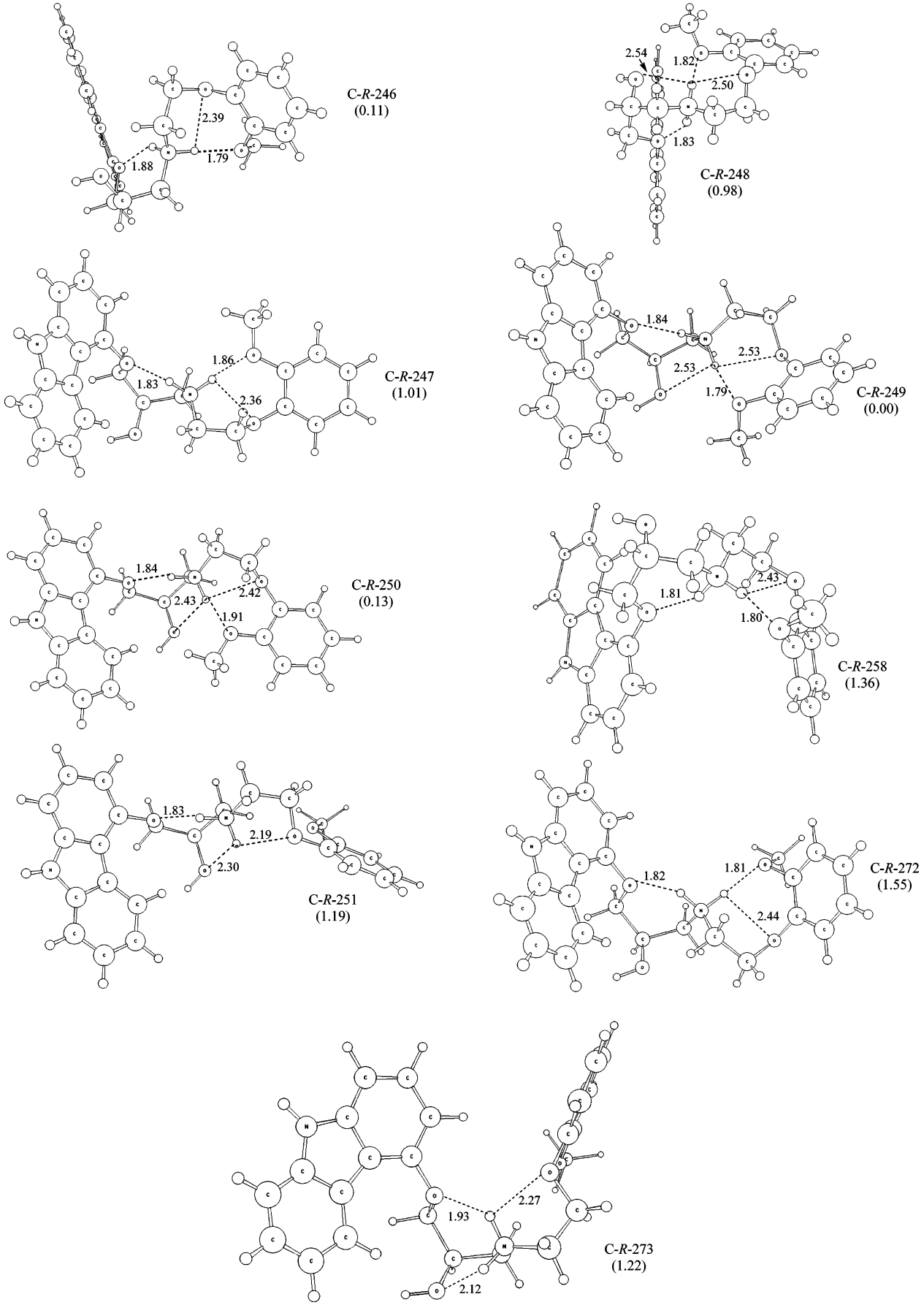

Figure 4. Molecular structures (and relative energies) of gas-phase B3LYP/6-31G(d) optimized carvedilol conformations (cf. Table 2 for optimized parameters). Note that seven (C-*R*-246 to C-*R*-250, C-*R*-258, and C-*R*-272) of the nine conformers possess the tetracentric motif (cf. section 3.1 in the Results and Discussion).

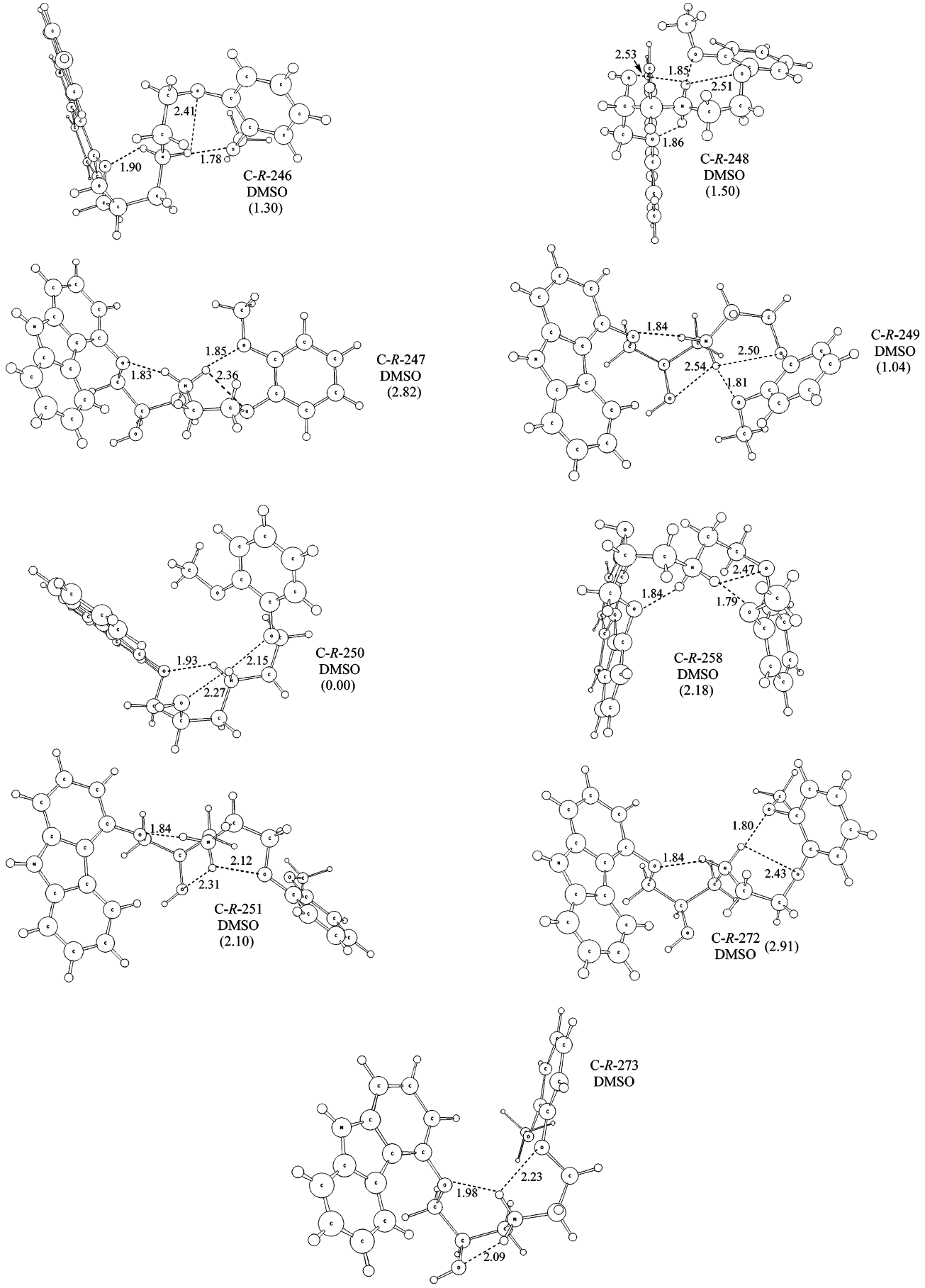

Figure 5. Molecular structures (and relative energies) of DMSO solvent phase B3LYP/6-31G(d) optimized carvedilol conformations (cf. Table 3 for optimized parameters).

TABLE 3: DMSO Optimized Values and Energies for the Converged Conformers of the Protonated *R*-Carvedilol Surface[a]

structure code	torsional angle (deg)											energy (hartree)	relative energy (kcal·mol^{-1})
	χ_1	χ_2	χ_3	χ_4	χ_5	χ_6	χ_7	χ_8	χ_9	χ_{10}	χ_{11}		
C-*R*-246	150.88	179.18	−63.08	67.55	92.89	−179.91	−48.08	−68.00	−69.15	60.25	92.98	−1340.99216696	1.30
C-*R*-247	108.63	−171.72	−55.13	66.64	84.64	108.06	−51.95	146.85	106.26	58.67	178.65	−1340.98974697	2.82
C-*R*-248	101.74	−171.19	−54.11	66.06	−172.30	−172.33	63.79	−126.92	−74.53	56.40	98.42	−1340.99185150	1.50
C-*R*-249	102.46	−172.21	−53.76	69.78	−162.90	−61.65	−47.65	−70.57	−69.72	54.54	92.88	−1340.99258309	1.04
C-*R*-250	91.13	−175.76	−51.32	73.87	177.54	−166.65	52.18	−162.59	−111.58	67.08	−176.93	−1340.99423903	0.00
C-*R*-251	104.99	−172.30	−52.94	71.61	−175.19	−71.24	−46.43	174.18	113.01	58.03	177.65	−1340.99089225	2.10
C-*R*-258	115.34	−174.34	−57.00	66.15	87.38	178.29	−60.89	114.39	70.11	65.18	−88.62	−1340.99075953	2.18
C-*R*-272	96.58	−175.49	−55.15	63.87	80.29	64.83	44.94	71.61	68.40	62.88	−94.46	−1340.98960067	2.91
C-*R*-273	98.22	177.38	−52.43	74.93	170.96	68.11	48.42	−177.80	−108.48	65.23	−172.71	−1340.99194603	1.44

[a] Structures were optimized using the Onsager (dipole) reaction field calculation model in DMSO ($\epsilon = 46.7$) at the B3LYP/6-31G(d) level of theory (cf. Table S1 for respective solute radii used in Onsager calculations).

stereocenter of carvedilol (torsional angle χ_{10}) indicating further inflexibility in the favored carvedilol conformations.

$$\chi_1 = g^+/a \quad \chi_6 = g^+/a/g^-$$
$$\chi_2 = a \quad \chi_7 = g^+/g^-$$
$$\chi_3 = g^- \quad \chi_8 = g^+/a/g^-$$
$$\chi_4 = g^+ \quad \chi_9 = g^+/g-$$
$$\chi_5 = g^+/a \quad \chi_{10} = g^+$$
$$\chi_{11} = g^+/a/g^- \qquad (3)$$

As shown in previous work on the enantiomeric relationships of carvedilol and fragment A,[15] the present results determined for the *R*-configuration of carvedilol can be extrapolated to predict corresponding energetic terms, conformational assignments, structural orientations, and IMAF of *S*-carvedilol. Since all carvedilol minima occur in analogous pairs,[15] the PEHSs for both stereoisomers will illustrate that the *R*- and *S*-configurations of carvedilol comprise a molecular system which possesses both point chirality and axis chirality and are exactly enantiomeric as described by eq 4. As a result, a true enantiomeric pair requires not only the switching of point chirality from the *R*- to *S*-stereoisomer but also the switching of all torsional angles from clockwise to counterclockwise rotation as demanded by eq 4. Thus, all minima must have an energetically equal enantiomer while all other carvedilol pairs have diastereomeric relationships.

$$E_R = E_S$$
$$f_R(\chi_1, \chi_2, \chi_3, \chi_4, \chi_5, \chi_6, \chi_7, \chi_8, \chi_9, \chi_{10}, \chi_{11}) = f_S(-\chi_1, -\chi_2, -\chi_3, -\chi_4, -\chi_5, -\chi_6, -\chi_7, -\chi_8, -\chi_9, -\chi_{10}, -\chi_{11}) \qquad (4)$$

3.4. NMR Spectroscopy of Carvedilol in DMSO Solvent. Carvedilol NMR chemical shifts and assignments are presented in Table 5. Initially, a ROESY spectrum was utilized to analyze the relatively rigid fragment A structure of carvedilol (i.e., about torsional angles χ_1, χ_2, χ_3, χ_4, and χ_5) (cf. eq 3). The ROESY spectrum shows that the carbazole proton H22 gives good intensity cross-peaks to nonequivalent H39 and H40 protons indicating that H22 is close to these two protons and that there is rigid motion about torsional angles χ_1, χ_2, and χ_3. Moreover, ROESY spectra also indicate that the H44 and H45 protons of center C25 are also not equivalent, and as a result, rotation about torsional angles χ_4 and χ_5 is likely hindered. Given these results, along with the fact that DMSO solvent generally destroys weak intramolecular H-bonding, the ROESY spectrum suggests that (1) the fragment A associated torsional angles of carvedilol are indeed inflexible and (2) the intramolecular H-bond networks present in the carvedilol structure are strong and persistent.

With reference to the theoretical DMSO optimized structures, all conformers possess at least one intramolecular H-bond involving an amine proton and the carbazole ether oxygen (O1) while conformers C-*R*-248, C-*R*-249, C-*R*-250, C-*R*-251, and C-*R*-273 contain a further H-bond between an amine proton and the hydroxyl oxygen (O41) (cf. Figure 5). These intramolecular H-bonds severely hinder any rotation involving torsional angles χ_1, χ_2, χ_3, χ_4, and χ_5. In addition, because the nitrogen center is protonated and further interacts (via H-bond formation) with oxygen atoms O29 and O36 bonded to the substituted benzene, further hindrance is placed on the rotation of these five torsional angles. As such, the ROESY spectra substantiates the DFT converged structures in that, given the various intramolecular H-bonds that carvedilol forms, it would be expected that protons H39 and H40 as well as H44 and H45 constitute nonequivalent centers.

Scalar coupling of protons H44 and H45 (C25 center) to proton H43 (stereocenter C24) was analyzed to closely inspect the behavior of torsional angle χ_4. Scalar coupling data with integration of NOE intensity curves reveals a large *J*-coupling value and corresponding large NOE intensity for proton H45 to proton H43 suggesting a dihedral value of ±60° (cf. Figure 8, left). Meanwhile, low J-coupling and low NOE values were observed for proton H44 to proton H43 implying a dihedral shift of 120° (cf. Figure 8, right).

DMSO optimized carvedilol conformers (cf. Figure 5) and their respective optimized parameters (cf. Table 3) reveal that all low energy carvedilol structures have torsional angle χ_4 in the g^+ orientation; the Newman projection in Figure 9 displays the g^+ orientation of torsional angle χ_4. In this gauche conformation, proton H45 imparts a large NOE and J-coupling influence to stereocenter proton H43 while proton H44 is shifted relative to torsional angle χ_4. Together, this conformation corroborates the NMR spectroscopy data.

The overlap signal and lack of NMR spectroscopic resolution concerning the aromatic benzene protons (H51, H52, H53, and H54) did not allow for any clear conclusions concerning the fragment C portion of the carvedilol structure. Overall, the NMR spectroscopy results closely mirror the optimized DFT structures and give full credibility to such high level gas and solvent phase calculations. Furthermore, as a whole, the theoretically and experimentally determined carvedilol structures are in extensive agreement and portray carvedilol as a relatively inflexible molecule with various robust IMAF.

Given the data, carvedilol does not seem to be susceptible to a large solvent effect (vs the gas phase) as its conformers are largely unchanged from gas to solvent phases; both the DFT

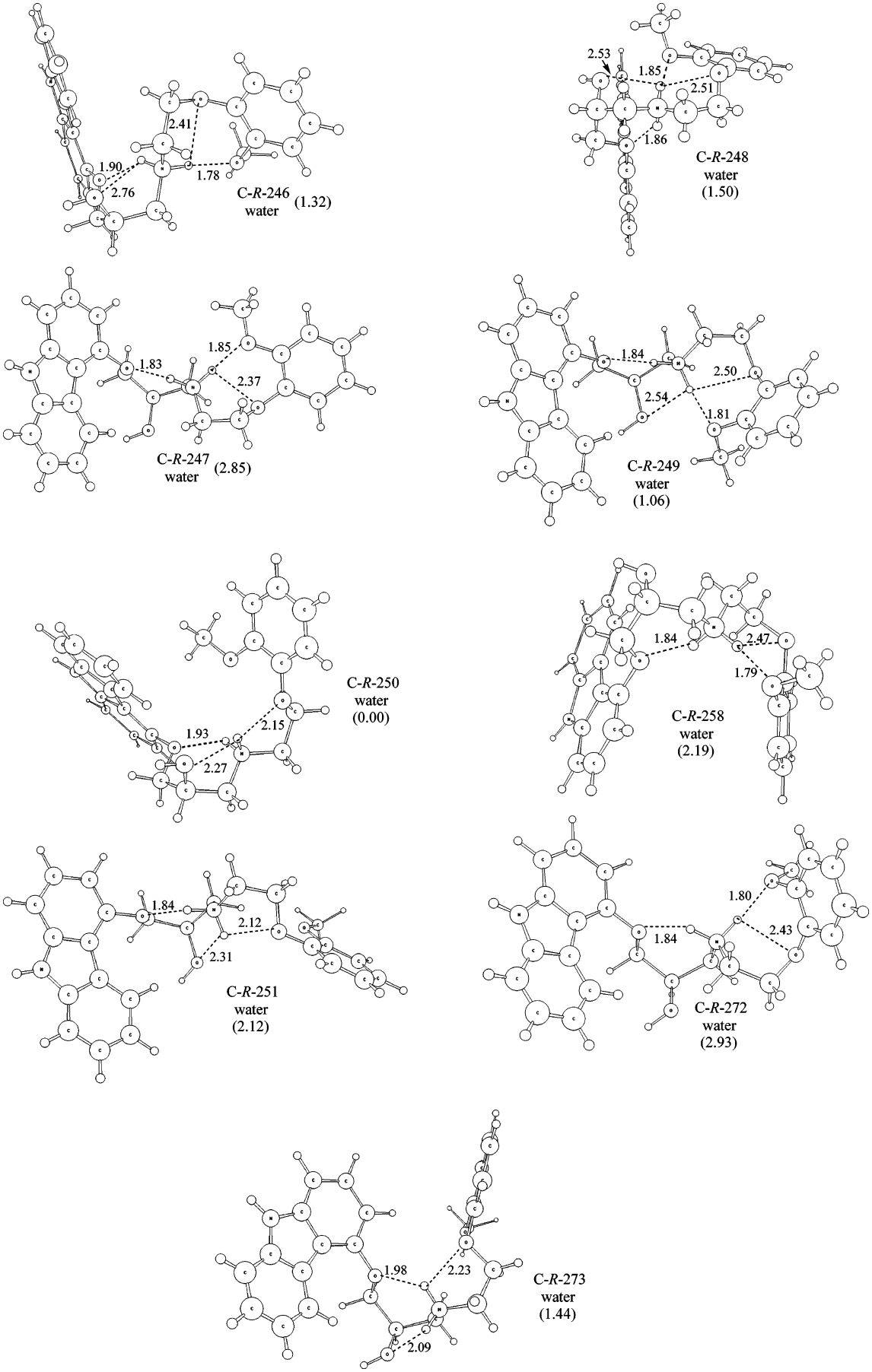

Figure 6. Molecular structures (and relative energies) of water solvent phase B3LYP/6-31G(d) optimized carvedilol conformations (cf. Table 4 for optimized parameters).

TABLE 4: Water Optimized Values and Energies for the Converged Conformers of the Protonated *R*-Carvedilol Surface[a]

structure code	torsional angle (deg)											energy (hartree)	relative energy (kcal·mol^{-1})
	χ_1	χ_2	χ_3	χ_4	χ_5	χ_6	χ_7	χ_8	χ_9	χ_{10}	χ_{11}		
C-*R*-246	150.84	179.18	−63.08	67.55	92.88	−179.87	−48.08	−68.01	−69.16	60.35	93.04	−1340.99219535	1.32
C-*R*-247	108.23	−171.74	−55.21	66.48	84.80	107.04	−51.55	146.70	106.37	58.30	178.53	−1340.98976077	2.85
C-*R*-248	101.82	−171.19	−53.92	66.10	−172.10	−171.98	63.68	−126.97	−74.48	56.51	98.38	−1340.99190386	1.50
C-*R*-249	102.19	−172.53	−53.48	69.90	−163.21	−62.04	−47.86	−70.22	−69.67	56.39	92.20	−1340.99261927	1.06
C-*R*-250	91.26	−175.77	−51.35	73.87	177.49	−166.72	52.19	−162.67	−111.57	67.18	−176.89	−1340.99430184	0.00
C-*R*-251	105.11	−172.31	−52.99	71.60	−175.21	−71.30	−46.43	174.16	113.05	58.12	177.61	−1340.99093123	2.12
C-*R*-258	114.80	−174.65	−57.11	66.04	86.98	178.26	−60.87	114.42	70.10	65.88	−88.43	−1340.99081121	2.19
C-*R*-272	96.56	−175.39	−55.28	63.90	80.69	64.73	44.89	71.69	68.43	62.40	−94.42	−1340.98962465	2.93
C-*R*-273	98.46	177.28	−52.58	74.95	170.94	68.52	48.46	−177.73	−108.50	65.62	−172.58	−1340.99200916	1.44

[a] Structures were optimized using the Onsager (dipole) reaction field calculation model in water ($\epsilon = 78.39$) at the B3LYP/6-31G(d) level of theory (cf. Table S1 for respective solute radii used in Onsager calculations).

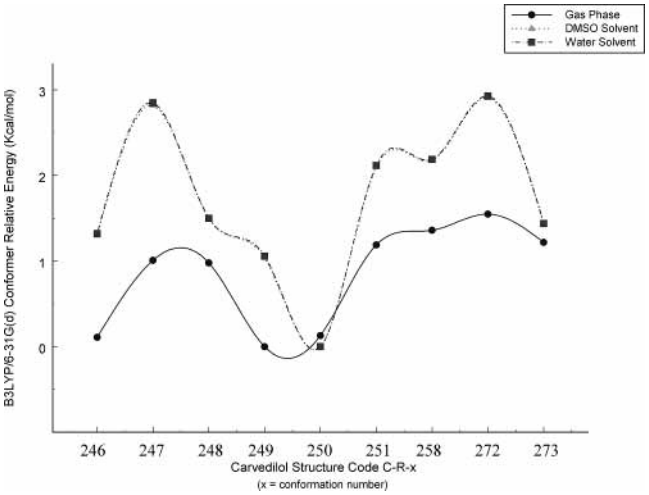

Figure 7. Graphical representation of the solvent effect of carvedilol. Gas, DMSO, and water phase relative energies are presented for all carvedilol structures optimized. Note that the DMSO and water relative energies extensively overlap each other due to near identical values (cf. section 3.2 in the Results and Discussion and Table 3 and 4).

TABLE 5: NMR Proton Chemical Shifts and Assignments for Carvedilol in DMSO (DMSO-d_6)

proton chemical shift (θ, ppm)	proton assignment	relevant section of carvedilol
8.27	H15[a]	carbazole aromatic ring
7.14	H16[a]	
7.35	H17[a]	
7.46	H18[a]	
11.26	H19	
7.1	H20[a]	
7.3	H21[a]	
6.7	H22[a]	
5.2	H42	stereocenter
4.19	H43	
4.15	H39,[a] H40[a]	connecting backbone
2.88	H44	
2.83	H45	
2.95	H47, H48	
4.01	H49,[a] H50[a]	
3.73	H38, H55, H56	methoxy group
unresolved ∼ 6.8−6.9	H51, H52, H53, H54	aromatic benzene ring

[a] Cross-checked with ref 30.

calculations and NMR spectra illustrate rigid intramolecular H-bonded structures able to withstand the solvent medium. Future directions to testing carvedilol's insensitivity to a solvent effect will focus on the following: (1) as stated above, solvent optimization of carvedilol with explicit treatment of solvent molecules to expose solute−solvent interactions, (2) analysis of vibrational spectra in polar aprotic (DMSO) and polar protic (water) solvents to compare and further test the rigidity (i.e., if similar spectra is present in different media) of converged minima, and (3) transition state localization and thermodynamic reaction profiling between gas-phase minima and explicit solvent phase minima to look at the energetic barriers for conformational states going from the gas phase to the solvent phase.

4. Conclusions

The DFT optimizations and NMR spectroscopy described here consist of the most detailed account of the electronic structure and significant conformational intricacies of carvedilol (e.g., tetracentric motif, IMAF, and H-bond networks) available

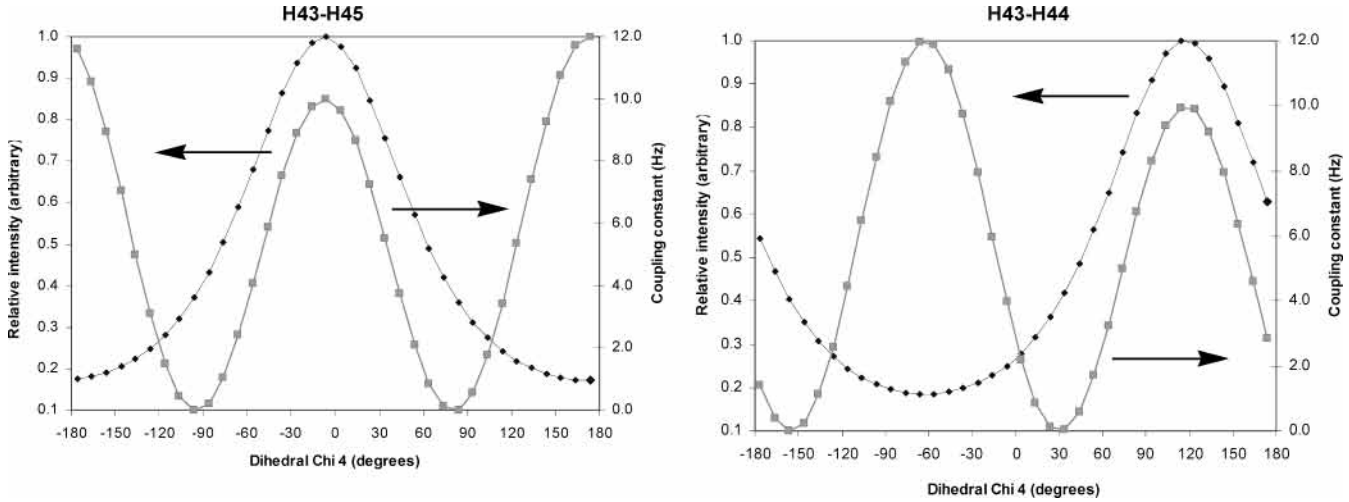

Figure 8. Graphical representation of the relationship between J-coupling and NOE intensity for protons H45 (left) and H44 (right) to stereocenter proton H43.

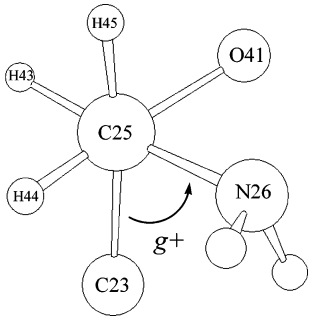

Figure 9. Newman projection of the g^+ orientation of carvedilol torsional angle χ_4.

in the literature. Carvedilol, although possessing significant conformational flexibility, also displays uncanny rigidity in several torsional angles (χ_1, χ_2, χ_3, χ_4, and χ_{10}). Given that these torsion dihedrals are respective to the aromatic carbazole centroid, it is likely that this region dictates the most prevalent and stable conformations of carvedilol. With regard to the solvent effect, DFT gas phase and Onsager solvent reaction field calculations (in DMSO and water) and NMR spectroscopy (in DMSO) closely parallel each other indicating carvedilol does not have an appreciable solvent effect. The elucidation and resolution of carvedilol's conformational character should greatly aid the molecular understanding of its cardiovascular active conformations and involvement with pathological molecular targets such as in oxidative stress and AD.

The rational molecular fragmentation method applied to carvedilol is as follows: if carvedilol, a molecule with many degrees of freedom (i.e., a large conformational hypersurface), is divided into simpler structural fragments (e.g., fragments A, B, and C) with manageable PEHSs but still relevant to the electronic structure of the whole molecule, then these smaller structures can be thoroughly analyzed via MDCA whereas carvedilol cannot. Then, the latter dominant fragment conformations, once optimized and evaluated, can be used to hypothesize low energy conformations of carvedilol itself. Since only highly populated fragment states are utilized, they should ultimately lead to corresponding low energy states of carvedilol.

Rather than relying on profligate computing force, this approach is in harmony with novel methodologies that localize dominant conformations of large PEHSs, not by means of sampling alone, but by designing routes that have the ability to generate starting points with some amount of energy minimization.[31] For example, the current fragmentation methodology does not sample the carvedilol map randomly, but rather, the fragments are optimized to generate inputs with an inherent amount of energy minimization.[17] The approach simplifies PEHS sampling because it is "focused" on conformers hypothesized to be highly populated states.[17]In this manner, the existing authors were successfully able to theoretically arrive at the low energy conformations of carvedilol that are presumed to dominate physical and biological samples via a novel methodological approach (i.e., rational molecular fragmentation method); the independent NMR spectroscopy results fully support these findings.

Acknowledgment. I.G.C. wishes to thank the Hungarian Ministry of Education for a Szent-Györgyi Visiting Professorship.

Supporting Information Available: Solute radius values. This material is available free of charge via the Internet at http://pubs.acs.org.

References and Notes

(1) Cheng, J.; Kamiya, K.; Kodama, I. *Cardiovasc. Drug Rev.* **2001**, *19*, 152.

(2) Carlson, W.; Oberg, K. *J. Cardiovasc. Pharmacol. Ther.* **1999**, *4*, 205.

(3) Capomolla, S.; Febo, O.; Gnemmi, M.; Riccardi, G.; Opasich, C.; Carporotondi, A.; Mortara, A.; Pinna, G.; Cobelli, F. *Am. Heart J.* **2000**, *139*, 596.

(4) Oliveira, P. J.; Marques, M. P.; Batista de Carvalho, L. A. E.; Moreno, A. J. M. *Biochem. Biophys. Res. Commun.* **2000**, *276*, 82.

(5) Howlett, D. R.; George, A. R.; Owen, D. E.; Ward, R. V.; Markwell, R. E. *Biochem. J.* **1999**, *343*, 419.

(6) Hardy, J.; Selkoe, J. *Science* **2002**, *297*, 353.

(7) Lee, V. M.-Y. *Neurobiol. Aging* **2002**, *23*, 1039.

(8) Walsh, D. M.; Klyubin, I.; Fadeeva, J. V.; Cullen, W. K.; Anwyl, R.; Wolfe, M. S.; Rowan, M. J.; Selkoe, D. J. *Nature (London)* **2002**, *416*, 535.

(9) Lambert, M. P.; Barlow, A. K.; Chromy, B. A.; Edwards, C.; Freed, R.; Liosatos, M.; Morgan, T. E.; Rozovsky, I.; Trommer, B.; Viola, K. L.; Wals, P.; Zhang, C.; Finch, C. E.; Krafft, G. A.; Klein, W. L. *Proc. Natl. Acad. Sci. U.S.A.* **1998**, *95*, 6448.

(10) Walsh, D. M.; Hartley, D. M.; Kusumoto, Y.; Fezoui, Y.; Condron, M. M.; Lomakin, A.; Benedek, G. B.; Selkoe, D. J.; Teplow, D. B. *J. Biol. Chem.* **1999**, *274*, 25945.

(11) Chui, D.-H.; Tanahashi, H.; Ozawa, K.; Ikeda, S.; Checler, F.; Ueda, O.; Suzuki, H.; Araki, W.; Inoue, H.; Shirotani, K.; Takahashi, K.; Gallyas, F.; Tabira, T. *Nature Med.* **1999**, *5*, 560.

(12) Almeida, D. R. P.; Pisterzi, L. F.; Chass, G. A.; Torday, L. L.; Varro, A.; Papp, J. Gy.; Csizmadia, I. G. *J. Phys. Chem. A* **2002**, *106*, 10423.

(13) Almeida, D. R. P.; Gasparro, D. M.; Pisterzi, L. F.; Torday, L. L.; Varro, A.; Papp, J. Gy.; Penke, B. *J. Mol. Struct. THEOCHEM* **2003**, *631*, 251.

(14) Almeida, D. R. P.; Gasparro, D. M.; Pisterzi, L. F.; Juhasz, J. R.; Fülöp, F.; Csizmadia, I. G. *J. Mol. Struct. THEOCHEM* **2003**, *666*−*667*, 557.

(15) Almeida, D. R. P.; Gasparro, D. M.; Pisterzi, L. F.; Torday, L. L.; Varro, A.; Papp, J. Gy.; Penke, B.; Csizmadia, I. G. *J. Phys. Chem. A* **2003**, *107*, 5594.

(16) Almeida, D. R. P.; Gasparro, D. M.; Pisterzi, L. F.; Juhasz, J. R.; Fülöp, F.; Csizmadia, I. G. *J. Mol. Struct. THEOCHEM* **2003**, *666*−*667*, 537.

(17) Almeida, D. R. P.; Gasparro, D. M.; Fülöp, F.; Csizmadia, I. G. *J. Phys. Chem. A* **2004**, submitted for publication.

(18) Frisch, M. J.; Trucks, G. W.; Schlegel, H. B.; Scuseria, G. E.; Robb, M. A.; Cheeseman, J. R.; Zakrzewski, V. G.; Montgomery, J. A., Jr.; Stratmann, R. E.; Burant, J. C.; Dapprich, S.; Millam, J. M.; Daniels, A. D.; Kudin, K. N.; Strain, M. C.; Farkas, O.; Tomasi, J.; Barone, V.; Cossi, M.; Cammi, R.; Mennucci, B.; Pomelli, C.; Adamo, C.; Clifford, S.; Ochterski, J.; Petersson, G. A.; Ayala, P. Y.; Cui, Q.; Morokuma, K.; Malick, D. K.; Rabuck, A. D.; Raghavachari, K.; Foresman, J. B.; Cioslowski, J.; Ortiz, J. V.; Baboul, A. G.; Stefanov, B. B.; Liu, G.; Liashenko, A.; Piskorz, P.; Komaromi, I.; Gomperts, R.; Martin, R. L.; Fox, D. J.; Keith, T.; Al-Laham, M. A.; Peng, C. Y.; Nanayakkara, A.; Gonzalez, C.; Challacombe, M.; Gill, P. M. W.; Johnson, B. G.; Chen, W.; Wong, M. W.; Andres, J. L.; Head-Gordon, M.; Reploglem, E. S.; Pople, J. A. Gaussian 98 (Revision A.9). Gaussian, Inc.: Pittsburgh, PA, 1998.

(19) Becke, A. D. *J. Chem. Phys.* **1993**, *98*, 5648.

(20) Wong, M. W.; Frisch, M. J.; Wiberg, K. B. *J. Am. Chem. Soc.* **1991**, *113*, 4776.

(21) Wong, M. W.; Wiberg, K. B.; Frisch, M. J. *J. Am. Chem. Soc.* **1992**, *114*, 523.

(22) Wong, M. W.; Wiberg, K. B.; Frisch, M. J. *J. Chem. Phys.* **1991**, *95*, 8991.

(23) Wong, M. W.; Wiberg, K. B.; Frisch, M. J. *J. Am. Chem. Soc.* **1992**, *114*, 4, 1645.

(24) Kirkwood, J. G. *J. Chem. Phys.* **1934**, *2*, 351.

(25) Onsager, L. *J. Am. Chem. Soc.* **1936**, *58*, 1486.

(26) Foresman, J. B.; Frish, A. Reaction field models of solvation. In *Exploring Chemistry with Electronic Structure Methods*, 2nd ed.; Gaussian Inc.: Pittsburgh, PA, 1996, pp 237−249.

(27) Axum 5.0C for Windows, MathSoft Incorporated, 1996.

(28) Excel for Windows, Microsoft, 2002.

(29) Chen, W.-M.; Zeng, L.-M.; Yu, K.-B.; Xu, J.-H. *Chin. J. Struct. Chem.* **1998**, *17*, 325.

(30) Schaeffer, W. H.; Politowski, J.; Hwang, B.; Dixon, F., Jr.; Goalwin, A.; Gutzait, L.; Anderson, K.; Debrosse, C.; Bean, M.; Rhodes, G. R. *Drug Metab. Dispos.* **1998**, *26*, 958.

(31) Billings, E. Molecular Modeling and Drug Design. In *Foye's Principles of Medicinal Chemistry*, 5th ed.; Williams, D. A., Lemke, T. L., Eds.; Lippincott Williams & Wilkins: New York, 2002; pp 68−85.